Simulation of polar stratospheric clouds in the specified dynamics version of the whole atmosphere community climate model

T. Wegner,[1] D. E. Kinnison,[2] R. R. Garcia,[2] and S. Solomon[3]

[1]   We evaluate the simulation of polar stratospheric clouds (PSCs) in the Specified Dynamics version of the Whole Atmosphere Community Climate Model for the Antarctic winter 2005. In this model, PSCs are assumed to form instantaneously at a prescribed supersaturation, with a prescribed size distribution and number density. We use satellite observations of the Antarctic winter 2005 of nitric acid, water vapor, and PSCs to test and improve this PSC parameterization. Cloud-Aerosol Lidar with Orthogonal Polarization observations since 2006 show that in both hemispheres, the dominant PSC type throughout the entire polar winter is a mixture of Nitric Acid Trihydrate (NAT) and Supercooled Ternary Solutions droplets, but typical assumptions about PSC formation in the model at a given supersaturation do not produce such a population of particles and lead to earlier removal of HNO_3 from the gas phase compared to observations. In our new PSC scheme, the formation of mixed PSCs is forced by only allowing a fraction of total available HNO_3 to freeze to NAT and the remaining part to form STS. With this approach, a mixture of both is present throughout the winter, in agreement with observations. This approach yields good agreement with observations in terms of temperature-dependent removal of gas-phase HNO_3 and irreversible denitrification. In addition to nitric acid containing PSCs, we also investigate ice PSCs. We show that the choice of required saturation ratio of water vapor for ice formation can significantly improve the calculated vertical distribution of water vapor and is required to produce good agreement with observations.

1.   Introduction

[2]   Widespread formation of polar stratospheric clouds (PSCs) occurs every year during the Antarctic winter. This type of cloud also commonly occurs during Arctic winters [*Pitts et al.*, 2009, 2011] but with higher variability compared to the Antarctic due to the interannual variability of the Arctic polar vortex. These clouds play an important role in the processes leading to the depletion of ozone in the lower stratosphere in polar spring. PSCs provide reaction sites on their surface for heterogeneous chemistry [*Solomon et al.*, 1986], and solid PSC particles can grow large enough to efficiently denitrify [*Fahey et al.*, 2001] and dehydrate [*Kelly et al.*, 1989] the lower stratosphere through sedimentation. Despite their importance, the composition and the formation mechanisms of PSCs are still not well understood [*Lowe and MacKenzie*, 2008]. Observations by the space-borne lidar Cloud-Aerosol Lidar with Orthogonal Polarisation (CALIOP) on the CALIPSO satellite [*Winker et al.*, 2009] indicate that most PSCs consist of a mixture of Supercooled Ternary Solution (STS) droplets and low particle number density Nitric Acid Trihydrate particles (NAT) [*Pitts et al.*, 2009]. These large NAT "rocks" are mainly responsible for denitrifying the stratosphere [*Fahey et al.*, 2001]. PSCs that are composed of HNO_3 containing particles are referred to as Type I. Type II PSCs are clouds composed of ice particles which, analogous to NAT causing denitrification, can cause a dehydration of the lower stratosphere by sedimentation.

[3]   Most current global models either form NAT instantaneously at a prescribed supersaturation with a fixed particle number density and shape of the size distribution, [e.g., *Kinnison et al.*, 2007; *Eyring et al.*, 2010] or simulate nucleation at a prescribed nucleation rate [e.g., *Grooß et al.*, 2005; *Davies et al.*, 2006; *Feng et al.*, 2011]. While both approaches can produce distributions of nitrogen in the lower stratosphere which are in general agreement with

[1]Institute of Energy and Climate Research - Stratosphere, Forschungszentrum Juelich, Juelich, Germany.
[2]Atmospheric Chemistry Division, National Center for Atmospheric Research, Boulder, Colorado, USA.
[3]Department of Earth, Atmospheric and Planetary Sciences, Massachusetts Institute of Technology, Cambridge, Massachusetts, USA.

Corresponding author: T. Wegner, Institute of Energy and Climate Research - Stratosphere, Forschungszentrum Juelich GmbH IEK-7, 52425 Juelich, Germany. (t.wegner@fz-juelich.de)

observations of gas-phase HNO_3 [*Grooß et al.*, 2005; *Eyring et al.*, 2010], recent studies [*Pitts et al.*, 2009; *Lambert et al.*, 2012] which combined simultaneous observations of gas-phase HNO_3 by the Microwave Limb Sounder (MLS) and particulate matter by CALIOP provide additional constraints on the development of PSCs on a vortex wide scale. We use these data to investigate the representation and composition of PSCs in the Specified Dynamics version of the Whole Atmosphere Community Climate Model (SD-WACCM) and the temperature dependence of the HNO_3/H_2O removal from the gas phase. We focus our analysis on the Antarctic winter 2005, which from a dynamical point of view can be regarded as a typical Antarctic winter. Since the interannual variability of the Antarctic vortex is small except during the spring vortex breakdown [*Waugh and Randel*, 1999], our conclusions are also valid for other Antarctic winters.

2. Model and Measurement Description

2.1. Specified Dynamics—Whole Atmosphere Community Climate Model

[4] The Whole Atmosphere Community Climate Model, Version 4 (WACCM4) is a fully interactive chemistry climate model, where the radiatively active gases affect heating and cooling rates and therefore dynamics [*Garcia et al.*, 2007; *Marsh et al.*, 2007; *Tilmes et al.*, 2007; *Eyring et al.*, 2010]. A new version of WACCM4 has been developed that allows the model to be run with "external" specified dynamical (SD) fields [*Lamarque et al.*, 2012]. This version of WACCM leads to an improved representation of atmospheric dynamics and temperatures for the study of specific years of observations, compared to its free running counterpart. These meteorological fields come from the NASA Global Modeling and Assimilation Office Modern-Era Retrospective Analysis for Research and Applications (MERRA) [*Rienecker et al.*, 2011]. Temperature, zonal and meridional winds, and surface pressure are used to drive the physical parameterizations that control boundary layer exchanges, advective and convective transport, and the hydrological cycle. In this study, the WACCM4 meteorological fields are relaxed toward the MERRA reanalysis fields using the approach described in *Kunz et al.* [2011].

[5] The chemical module of WACCM4 is based upon the 3-D chemical transport Model of Ozone and Related Tracers, Version 3 (MOZART) [*Kinnison et al.*, 2007]. It includes a detailed representation of the chemical and physical processes from the troposphere through the lower thermosphere. The species included within this mechanism are contained within the O_x, NO_x, HO_x, ClO_x, and BrO_x chemical families, along with CH_4 and its degradation products. In addition, 14 primary nonmethane hydrocarbons and related oxygenated organic compounds are included [*Emmons et al.*, 2010]. This module contains 125 species, 253 gas-phase reactions, 75 photolytic processes, and 18 heterogeneous reactions on multiple aerosol types.

[6] The SD-WACCM/MERRA simulations analyzed in this study correspond to the time period from 1 May 2005 through 1 November 2005. The initialization for our simulations was derived from a SD-WACCM/MERRA simulation that started in January 1988 and ran through April 2005. The horizontal resolution is $1.9° \times 2.5°$, with a vertical resolution of <1 km in the troposphere, 1 km in the lower stratosphere, and about 2 km in the upper stratosphere. To allow for a direct comparison with satellite data, the model is sampled at the grid point and time step that are closest to the observations. This results in a maximum deviation of $0.95° \times 1.25°$ and 15 min between sampled model profile and observation.

[7] To describe the position of an air mass relative to the center of the vortex, we use equivalent latitude (EqL) as a spatial coordinate [*Butchard and Remsberg*, 1986]. Equivalent latitude describes the area encircled by a potential vorticity (PV) contour. Equivalent latitude is calculated from the PV field of the model output on the regular grid at 12 UTC each day and subsequently linearly interpolated to the measurement locations of the specific day. No interpolation in time is performed.
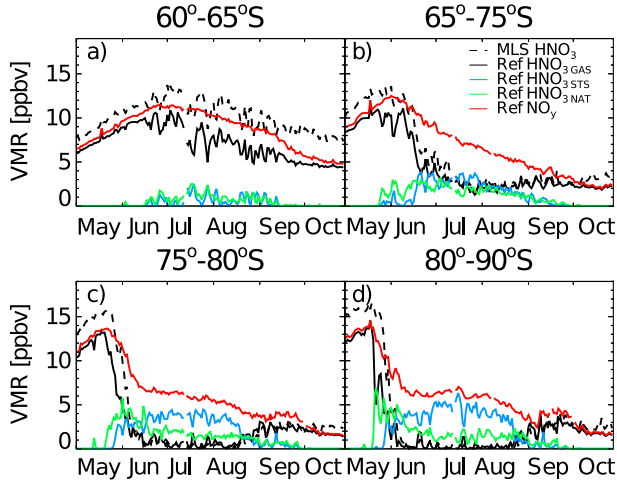
[8] To simulate PSCs, the reference SD-WACCM simulation uses an equilibrium approach to simulate NAT particles. STS is simulated according to the thermodynamic equilibrium model by *Tabazadeh et al.* [1994] with a particle number density of 10 cm^{-3} [*Dye et al.*, 1992]. Since observations [*Peter et al.*, 1991] show that a certain supersaturation is needed before NAT forms, we simulate the formation of NAT at a supersaturation of 10, about 3 K below its thermodynamic equilibrium temperature [*Hanson and Mauersberger*, 1988], at a prescribed particle number density of 10^{-1} cm^{-3}. This particle number density was chosen so that irreversible denitrification in the model agrees with observations. The background aerosol, STS, and NAT follow a lognormal size distribution with a width σ of 1.6 [*Kinnison et al.*, 2007]. The thermodynamic equilibrium temperature for NAT is referred to as T_{NAT}, and the temperature at a supersaturation of 10 is referred to T_{S_NAT}.

[9] For typical stratospheric conditions (50 hPa, 5 ppmv H_2O, 15 ppbv HNO_3), T_{NAT} and T_{S_NAT} correspond to $\sim$196 K and $\sim$193 K, respectively. In our analysis, we calculate these threshold temperatures for the conditions in the polar vortex at the beginning of winter before any denitrification or dehydration occurs, since we want to show to what extent these threshold temperatures can describe the actual beginning of the PSC phase.

[10] In the reference case, it is assumed that if atmospheric conditions allow the presence of either particle type, HNO_3 is preferably partitioned into STS (i.e., STS dominates at low temperatures). This PSC scheme does not take into account the history of the air. For given ambient conditions, the PSC scheme will always calculate exactly identical partitioning of HNO_3 between the gas phase, NAT, and STS regardless of whether the air mass is cooling or warming.

2.2. Microwave Limb Sounder

[11] The Microwave Limb Sounder (MLS) is an instrument on the EOS Aura satellite which is in a polar orbit of 705 km at an inclination of $98°$, and has provided continuous measurements since 2004 [*Waters et al.*, 2006]. MLS provides about 3500 profiles from Earth's surface to 90 km altitude between $82°$N and $82°$S. We use observations of gas-phase HNO_3 [*Santee et al.*, 2007], H_2O [*Lambert et al.*, 2007], and temperature [*Schwartz et al.*, 2008] from retrieval version 3.3. The vertical resolution and precision of the observations are 3.5–4.5 km and 0.7 ppbv for HNO_3; 3 km and 15% for H_2O; and 4 km and 1 K for temperature.

Figure 1. Daily averaged MLS observations of gas-phase HNO_3, modeled NO_y (total) and modeled partitioning of HNO_3 between the gas phase, NAT, and STS on 475 K over Antarctica 2005 for four equivalent latitude regions. NO_y shows the irreversible denitrification over the course of the winter. Dashed lines are observations of gas-phase HNO_3 by MLS, and solid lines model output from the reference simulation. Ticks on the x-axis mark the first of each month, likewise in the following figures.
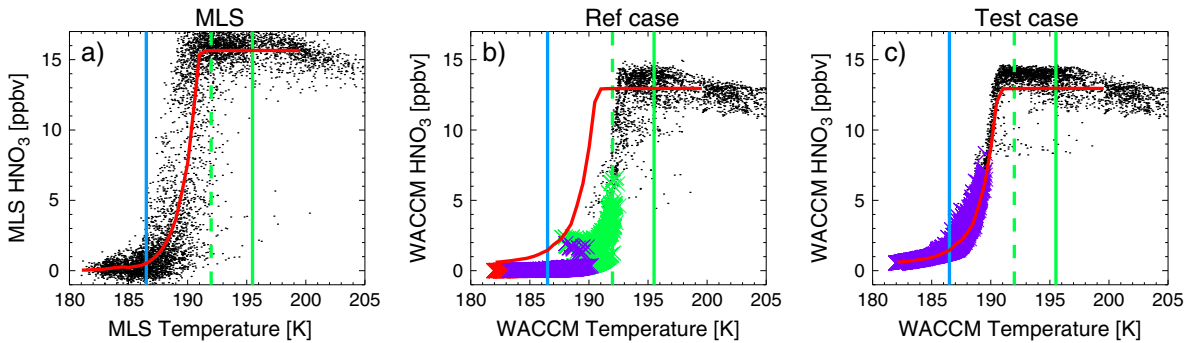
3. Type I PSCs
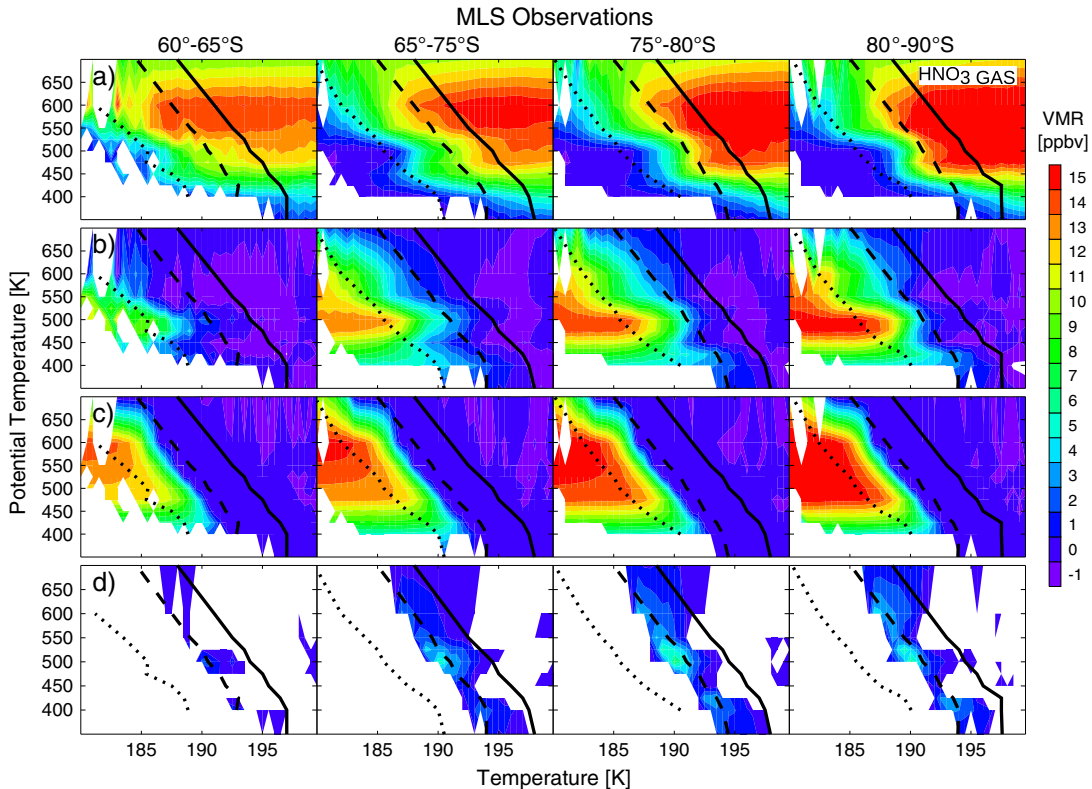
3.1. Observations and Reference Simulation

[12] Figure 1 shows the typical development of HNO_3 containing species in the reference simulation and observations of gas-phase HNO_3 by MLS on the 475 K potential temperature surface in volume mixing ratio (VMR). The initial increase in gas-phase HNO_3 is caused by descent of HNO_3-rich air masses, but with decreasing temperatures, the model forms PSCs which rapidly deplete gas-phase HNO_3. In the reference model, NAT is formed first, and then transitions into STS as temperatures decrease further. This is most evident in the vortex core (Figure 1d). As soon as the temperature threshold, T_{S_NAT}, for NAT is reached, gas-phase HNO_3 drops sharply as HNO_3 is partitioned into NAT. As temperatures decrease further, STS starts to form and quickly becomes the prevalent PSC type. This indicates that in the reference simulation, HNO_3 sequestered within PSCs transitions from the solid to the liquid phase with decreasing temperature. This transition is not supported by observations which show that STS droplets are the first PSC type to form [e.g., *Pitts et al.*, 2011].

[13] Model and observations agree that HNO_3 is nearly completely removed from the gas phase throughout the entire winter poleward of 80°S EqL and strongly depleted between 65°S and 80°S EqL. With the reference PSC scheme, most of the irreversible denitrification in the model, through the sedimentation of NAT particles, occurs in early winter as can be seen by the steep decline of total inorganic nitrogen (NO_y). NO_y describes the inorganic nitrogen content in all three phases: gas, liquid, and solid. By the middle of June, about 50% of total modeled irreversible denitrification in the vortex core has already occurred. Once HNO_3 is partitioned into STS in the model, NO_y decreases more gradually. At very low temperatures when almost all available HNO_3 in the model is partitioned into STS, further irreversible denitrification stops as shown by constant NO_y in July in the vortex core (Figure 1d). Farther away from the vortex core, the formation of NAT in the model is less abrupt. The model shows that STS and NAT start to form at about the same time, and HNO_3 is equally distributed between STS, NAT, and the gas phase. This leads to more gradual denitrification but reaches the same extent as simulated in the vortex core at the end of the Antarctic winter (Figure 1b).

Figure 2. (a) All MLS gas-phase HNO_3 observations on 475 K between 1 May and 1 July 2005 poleward of 80°S EqL over Antarctica correlated with temperature. (b) Reference simulation output co-located with the observations described in Figure 2a. (c) Same as Figure 2b for the test simulation. Green marks PSCs mainly composed of NAT, with more than 50% of total HNO_3 in NAT and less than 10% in STS; Red PSCs with high STS content, more than 50% of HNO_3 in STS and less than 10% in NAT; and purple-mixed PSCs with more than 15% HNO_3 in NAT and more than 15% in STS. The red line marks the thermodynamic equilibrium for STS particles, calculated according to *Carslaw et al.* [1995a]. Solid green line marks T_{NAT}, dashed green line T_{S_NAT}, and solid blue T_{ICE}. These threshold temperatures are calculated with the mean HNO_3 and H_2O concentrations between 195 and 200 K on the 475 K isentrope poleward of 80°S EqL, separately for observations and the model simulations.
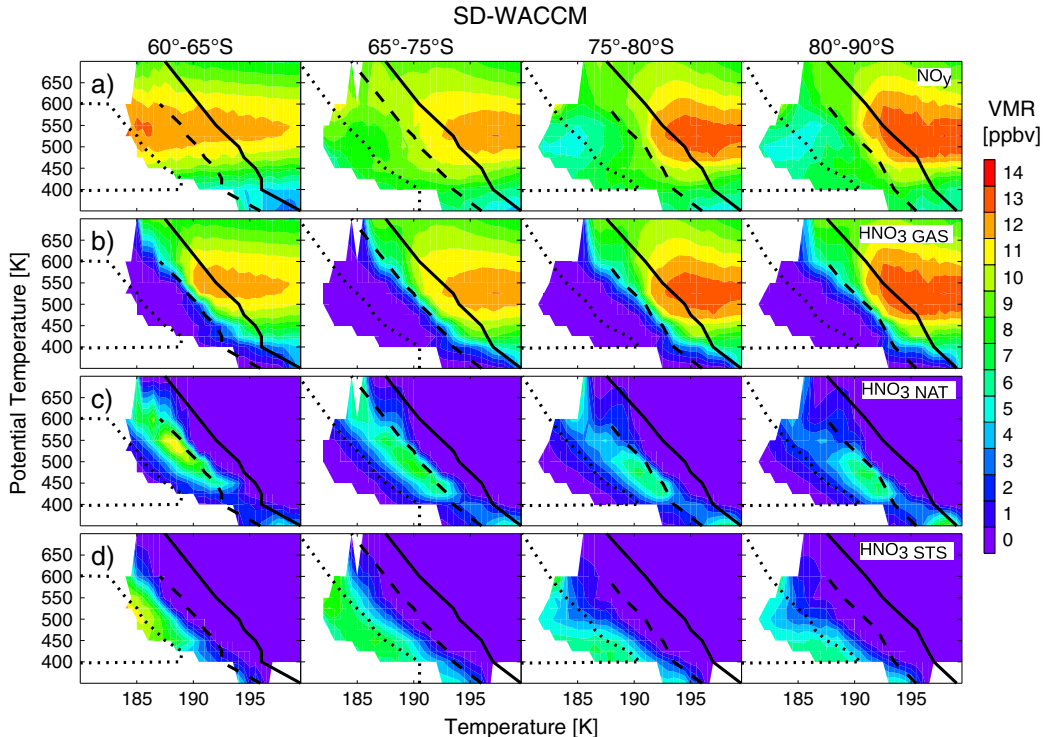
3

Figure 3. (a) All vertical profiles of MLS gas-phase HNO_3 observations between 1 May to 1 July 2005 averaged in 1 K temperature intervals for four equivalent latitude regions in potential temperature space. (b) Difference between the observed vertical distribution of HNO_3 at a given temperature, shown in row of Figure 3a, and the initial distribution. Initial HNO_3 is the mean vertical distribution of gas-phase HNO_3 between 195 and 200 K temperature. (c) Theoretical uptake of HNO_3 by STS, calculated according to *Carslaw et al.* [1995a]. Water vapor for this calculation is taken from MLS observations at a given temperature (Figure 9a) and HNO_3 from the observed initial mean vertical distribution between 195 and 200 K. (d) Difference of (b) observed HNO_3 removal from the gas phase and (c) theoretical uptake by STS; hence, removed gas-phase HNO_3 that cannot be explained with the theoretical uptake on STS. Solid line marks T_{NAT}, dashed T_{S_NAT}, and dotted T_{ICE}. These threshold temperatures are calculated separately at each altitude level and equivalent latitude region with mean MLS HNO_3 and H_2O concentrations between 195 and 200 K.

[14] CALIOP [*Pitts et al.*, 2009] and ground-based lidar [*Adriani et al.*, 2004] observations on the other hand indicate that the first PSCs formed are predominantly STS rather than NAT and that mixed phase PSCs exist through the entire winter, which suggests that denitrification is a more gradual process. The reference simulation cannot represent this gradual denitrification process in the vortex core. In the vortex edge region between 60°S and 65°S equivalent latitude (Figure 1a), PSCs are only present to a minor extent in the reference simulation, and most HNO_3 remains in the gas phase so that only minor denitrification occurs. Nonetheless, the overall modeled gas-phase HNO_3 and denitrification at the end of polar winter are in excellent agreement with observations of gas-phase HNO_3 by MLS. Poleward of 75°S EqL, observations also show total depletion of gas-phase HNO_3 and in the vortex edge region; between 65°S and 75°S EqL, gas-phase HNO_3 stays constant at low values.

[15] *Lambert et al.* [2012] have shown that MLS observations of gas-phase HNO_3 as a function of temperature can be used to evaluate the PSC type. In Figure 2, we correlate observations of gas-phase HNO_3 with temperature and compare this to MLS observations. We show all observations in May and June 2005 poleward of 80°S EqL on 475 K in the Antarctic. During this time, the vortex starts to form, gradually cools down, and observations indicate a decrease of gas-phase HNO_3 with decreasing temperatures (Figure 2a). If it is assumed that temperatures decrease rather monotonically throughout the vortex core, then the highest temperature at which a decrease in HNO_3 can be observed coincides with the formation of PSCs. In the observations, gas-phase HNO_3 starts to decrease near T_{S_NAT} and is completely depleted when temperatures reach the frost point. This decrease appears to follow the STS equilibrium function (Figure 2a, red line). We cannot be certain of the reasons for the scatter around this function, but contributing factors likely include the presence of mixed PSCs (solid and liquid) and the accuracy of the observations.

[16] The reference simulation of SD-WACCM differs significantly from the observations (Figure 2b). In the model, gas-phase HNO_3 shows a sharp drop at T_{S_NAT} and

Figure 4. All vertical profiles of the reference simulation between 1 May to 1 July 2005 averaged in 1 K temperature intervals for four equivalent latitude regions in potential temperature space. (a) Reference simulation NO_y (gas+condensed phase) between 180–200 K temperature and 300–700 K potential temperature. (b) Same as Figure 4a for modeled gas-phase HNO_3. (c) Same as Figure 4a for modeled HNO_3 in NAT. (d) Same as Figure 4a for modeled HNO_3 in STS. Solid line marks T_{NAT}, dashed T_{S_NAT}, and dotted T_{ICE}, calculated as described for Figure 3 with model HNO_3 and H_2O.
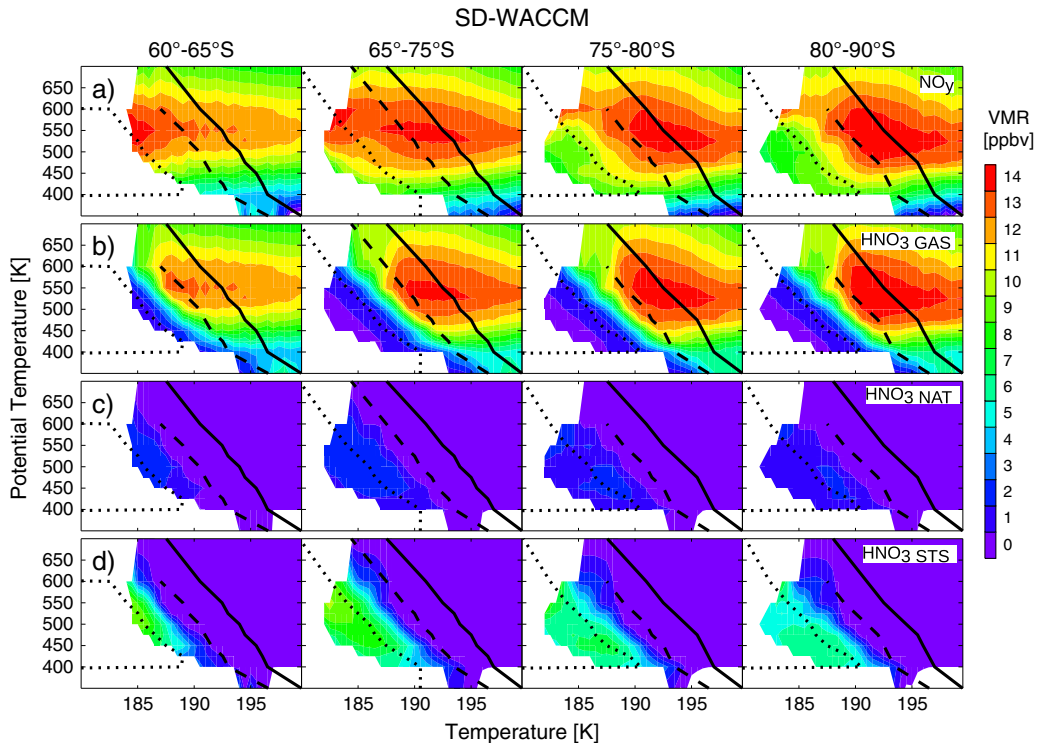
HNO_3 is completely removed from the gas phase between T_{S_NAT} and T_{ICE}. Once completely removed from the gas phase, only the partitioning of HNO_3 between the different PSC types changes as temperatures decrease further. *Lambert et al.* [2012] have shown that mixed clouds occur over the whole temperature range, simultaneous with residual gas-phase HNO_3. In the model, mixed PSCs only occur between $T_{ICE}-3$ K and $T_{ICE}+3.5$ K and gas-phase HNO_3 is completely depleted. At higher temperatures, modeled PSCs consist only of NAT and at lower only of STS particles. *Lambert et al.* [2012] have also shown that combined CALIOP and MLS observations of liquid PSCs follow the thermodynamic equilibrium function for STS. No model data points coincide with this function, since STS only forms after gas-phase HNO_3 has already been completely depleted by the preceding formation of NAT.

[17] Observations of the entire vortex show a similar dependence of gas-phase HNO_3 on temperature as the 475 K isentrope shown in Figure 2a. Initial removal of HNO_3 from the gas phase starts between T_{NAT} and T_{S_NAT} and reaches its maximum around T_{ICE} (Figure 3b). Using the STS equilibrium function from *Carslaw et al.* [1995a], we calculate the theoretical maximum uptake of HNO_3 on STS (Figure 3c). This theoretically possible uptake starts between T_{S_NAT} and T_{ICE}, and Figure 3d shows the difference between observed removal of gas-phase HNO_3 and the theoretical uptake by STS. Removal of HNO_3 before the uptake by STS may be due to the formation of NAT particles

(Figure 3d). Assuming that this decrease is caused by NAT particles, NAT formation begins at temperatures around T_{S_NAT} between 500 and 550 K. Outside this area, depletion of gas-phase HNO_3 can be explained by the presence of STS.

[18] The temperature-dependent transition between the different PSC types in the reference simulation shows significant differences compared to observations. In the model, gas-phase HNO_3 drops sharply as soon as the specified supersaturation, T_{S_NAT}, for NAT is reached (Figure 4b). Unlike the observations, which only provide gas-phase HNO_3, the partitioning between gas-phase HNO_3 and HNO_3 that is condensed to STS and NAT is exactly known in the model. At T_{S_NAT}, the model partitions all available HNO_3 into NAT without forming any STS (Figure 4c). When temperatures decrease further, STS becomes more abundant and below the frost point; STS is the dominant PSC type present (Figure 4d). This is contrary to the PSC behavior described in *Pitts et al.* [2009]. *Pitts et al.* [2009] show that STS forms first and transitions into mix 2 PSCs (STS and high particle number density NAT) as temperatures decrease. With increasing temperatures at the end of winter, mix 2 transitions back into STS. *Pitts et al.* [2009] do not report a transition from NAT to STS with decreasing temperature.

[19] Mixed PSCs only exist to a minor extent in the reference model between T_{S_NAT} and T_{ICE}. In the model, denitrification occurs in this narrow temperature range and shuts off when temperatures reach the frost point as NAT is no longer present. This behavior is not supported by

Figure 5. Same as Figure 4 for the test simulation with the improved PSC scheme. (a) Mean vertical distribution of NO_y (gas+condensed phase) as function of temperature. (b) Same as Figure 5a for modeled gas-phase HNO_3. (c) Same as Figure 5a for modeled HNO_3 in NAT. (d) Same as Figure 5a for modeled HNO_3 in STS. Solid line marks T_{NAT}, dashed T_{S_NAT}, and dotted T_{ICE}, calculated as described in Figure 4.

observations. Nonetheless, denitrification is very efficient in this simulation, with NO_y dropping from 12 to 6 ppbv between the beginning of May to the end of June in the vortex core on the 475 K isentrope once temperatures have reached the frost point. When temperatures in the vortex core increase again in August, HNO_3 is partitioned from STS into NAT, and irreversible denitrification continues.
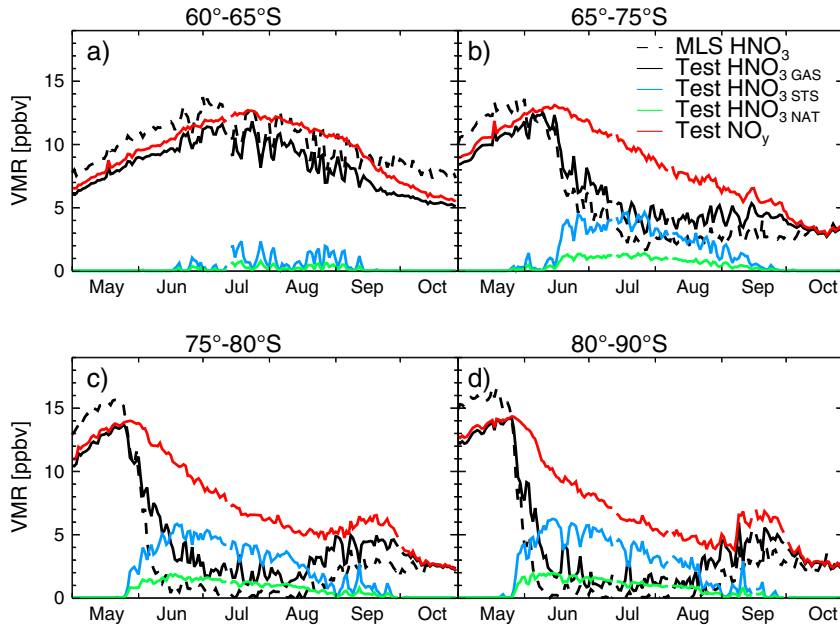
[20] From the comparison of modeled and observed gas-phase HNO_3, we conclude that the model represents the overall irreversible denitrification fairly well. By October, when the PSC phase ends and the remaining condensed HNO_3 is released back into the gas phase, observations and model agree that over the course of the winter, only 3 ppbv HNO_3 remain at this altitude. This is an important factor since the abundance of gas-phase HNO_3 can influence the speed of chlorine deactivation and therefore the extent of ozone depletion. However, the model's representation of HNO_3 containing PSCs is very different from the observations, since it hardly has any mixed phase PSCs and an unphysical transition from solid to liquid particles with decreasing temperatures.

3.2. PSC Type I Test Simulation with an Improved PSC Scheme

[21] Due to the unrealistic parameterization for the formation of NAT PSCs in the reference simulation that neither agrees with theory nor observations, we conduct a test case in which we change the way the model partitions HNO_3 between the different PSC types. CALIOP

observations suggest that most mixed phase PSCs occur at backscatter and depolarization ratios between the *Pitts et al.* [2009] classification of mix 1 and mix 2. Mix 1 clouds are composed of STS and low particle number density NAT (3×10^{-4} cm^{-3} to 10^{-3} cm^{-3}), and mix 2 of STS and high particle number density NAT ($> 10^{-3}$ cm^{-3}). The boundary between mix 1 and mix 2 corresponds to clouds containing NAT particles with an effective radius between 2 μm and 7 μm, and a particle number density between 10^{-2} cm^{-3} and 10^{-3} cm^{-3}. If we assume a NAT particle density of 1.62 g cm^{-3} [*Drdla et al.*, 1993], then between 2 and 10 ppbv HNO_3 are present in NAT. This corresponds to 15–75% of the total available HNO_3, assuming no irreversible denitrification. In addition, *Biele et al.* [2001] found that ground-based lidar observations of PSCs over Ny Ålesund (located at 79°N) can best be explained by assuming that only 5% of the total available HNO_3 is allowed to condense onto solid particles.

[22] In the test simulation of SD-WACCM, we therefore limit the amount of HNO_3 that is allowed to be present in NAT. We found that best agreement with observed denitrification in October, when the PSC phase has ended, is achieved when 20% of total available HNO_3 is allowed to form NAT at a supersaturation of 10 and a NAT particle number density of 10^{-2} cm^{-3}, essentially forming mix 2 PSCs in the model. Such a particle number density is also in better agreement with CALIOP observations than the 10^{-1} cm^{-3} which are assumed in the reference case, since *Pitts et al.* [2009, 2011] show that most NAT PSCs have a

Figure 6. Daily averaged MLS observations of gas-phase HNO_3, modeled NO_y (total), and modeled partitioning of HNO_3 between the gas phase, NAT, and STS on 475 K over Antarctica 2005 for four equivalent latitude regions. NO_y shows the irreversible denitrification over the course of the winter. Dashed lines are observations of gas-phase HNO_3 by MLS, and solid lines model output from the test simulation with the improved PSC scheme.

particle number density between 10^{-2} and 10^{-3} cm^{-3}. The composition of STS droplets is still calculated according to *Tabazadeh et al.* [1994], but only HNO_3 that has not been taken up by NAT is allowed to form STS.
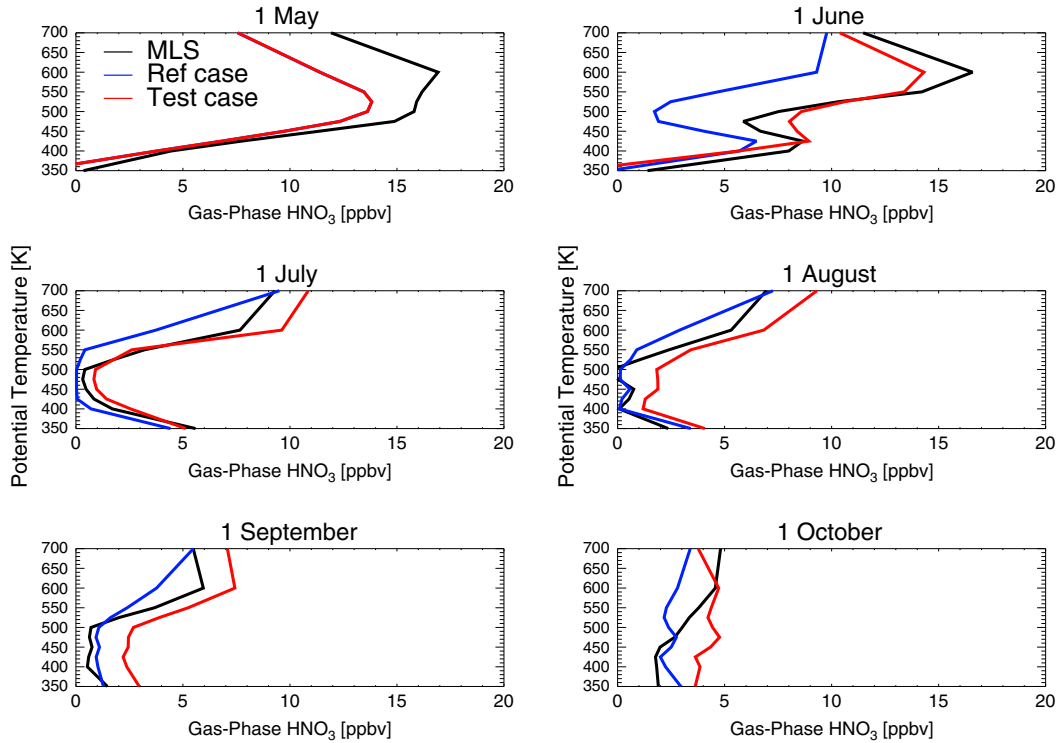
[23] With this approach, NAT PSCs occur at T_{S_NAT}; but instead of transitioning into STS with decreasing temperature, both PSC types can coexist throughout the entire temperature range, with STS becoming more abundant at lower temperatures (Figure 5c and 5d). This is consistent with *Carslaw et al.* [1994] who showed that the temperature dependence of in situ observations of PSCs agrees with a thermodynamic equilibrium model for STS and *Lambert et al.* [2012], who have shown that liquid PSCs still commonly occur at temperatures around the frost point. While the reference simulation shows a sharp drop in gas-phase HNO_3 when it is partitioned into NAT at T_{S_NAT}, HNO_3 is now gradually removed from the gas phase beginning at T_{S_NAT} and completely removed around the frost point (Figure 5b).

[24] The model still cannot reproduce the sharp decrease observed at 190 K around 500 K potential temperature (compare Figure 3a versus 5). *Pitts et al.* [2009] show increases in mix 2 PSCs at the beginning of June around 20 km, which would be consistent with this observed removal of HNO_3 from the gas phase, which could be driven by the formation of PSCs with high NAT particle number density. Since this decrease occurs over a very narrow temperature range and hence a short time frame, it is unlikely that this decrease is caused by the formation of large NAT particles with low particle number densities. Such large particles would need significant time to grow to deplete gas-phase HNO_3. Since the model forms NAT at only one prescribed number density and one specified

supersaturation, this behavior cannot be represented with the current PSC scheme.

[25] The temperature dependence of HNO_3 on the 475 K isentrope now shows better agreement with the observations (Figure 2c). Gas-phase HNO_3 now follows the STS equilibrium function, in good agreement with observations. The removal of HNO_3 from the gas phase is more compact than the reference simulation, and the sharp drop at T_{S_NAT} has been removed. However, a significant portion of HNO_3 (>15%) is present in NAT which leads to the occurrence of mixed PSC clouds. The model shows significantly less scatter than the satellite observations due to the simplification that all PSCs form instantaneously with a prescribed size distribution. In the real atmosphere, an air parcel's history, especially the cooling rate, will have a crucial influence on PSC composition and size distribution so that air masses sampled at the same temperature can have a very different partitioning of HNO_3 between gas phase and the different PSC types and do not necessarily have to be in thermodynamic equilibrium [*Meilinger et al.*, 1995].

[26] In the test case, denitrification is a continuous process, illustrated by the decrease in NO_y, which slows down gradually as HNO_3 is irreversibly removed from the lower stratosphere (Figure 6). There is little difference in terms of partitioning between gas phase, STS, and NAT between the different equivalent latitude regions poleward of 65°S. From the end of May onward, 20% of total available HNO_3 (the maximum amount allowed in the updated PSC scheme) is partitioned into NAT for almost 4 months poleward of 65°S equivalent latitude. Gas-phase HNO_3 is never completely removed, and throughout the winter, it is about 1–2 ppbv higher than observations. Still, irreversible denitrification in the test simulation in October is similar to the reference
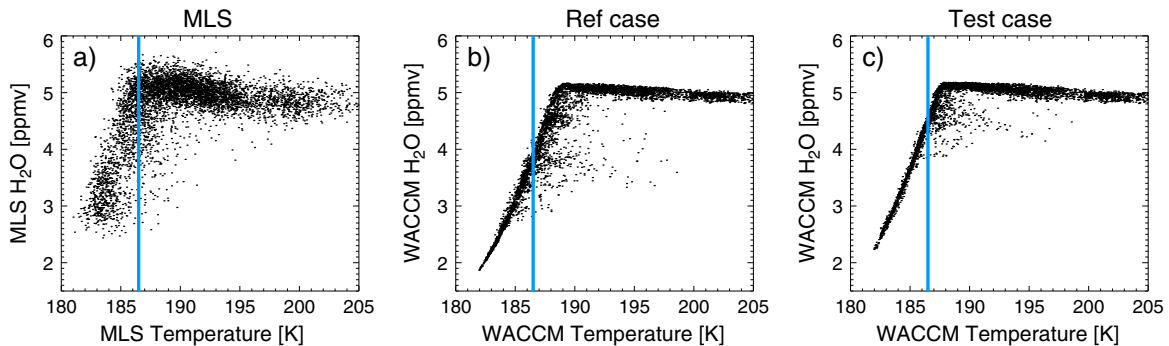
Figure 7. Average vertical profiles of gas-phase HNO_3 for six different days in 2005 poleward of 80°S EqL. Solid black lines are MLS measurements, blue lines are the reference simulation, and red lines are the test simulation with improved PSC scheme.

simulation and in good agreement with observations. Especially good agreement with observations is achieved for the initial decrease of gas-phase HNO_3 at the end of May. The new PSC scheme gives an excellent account of this observed decrease since it now occurs due to the formation of STS instead of NAT.
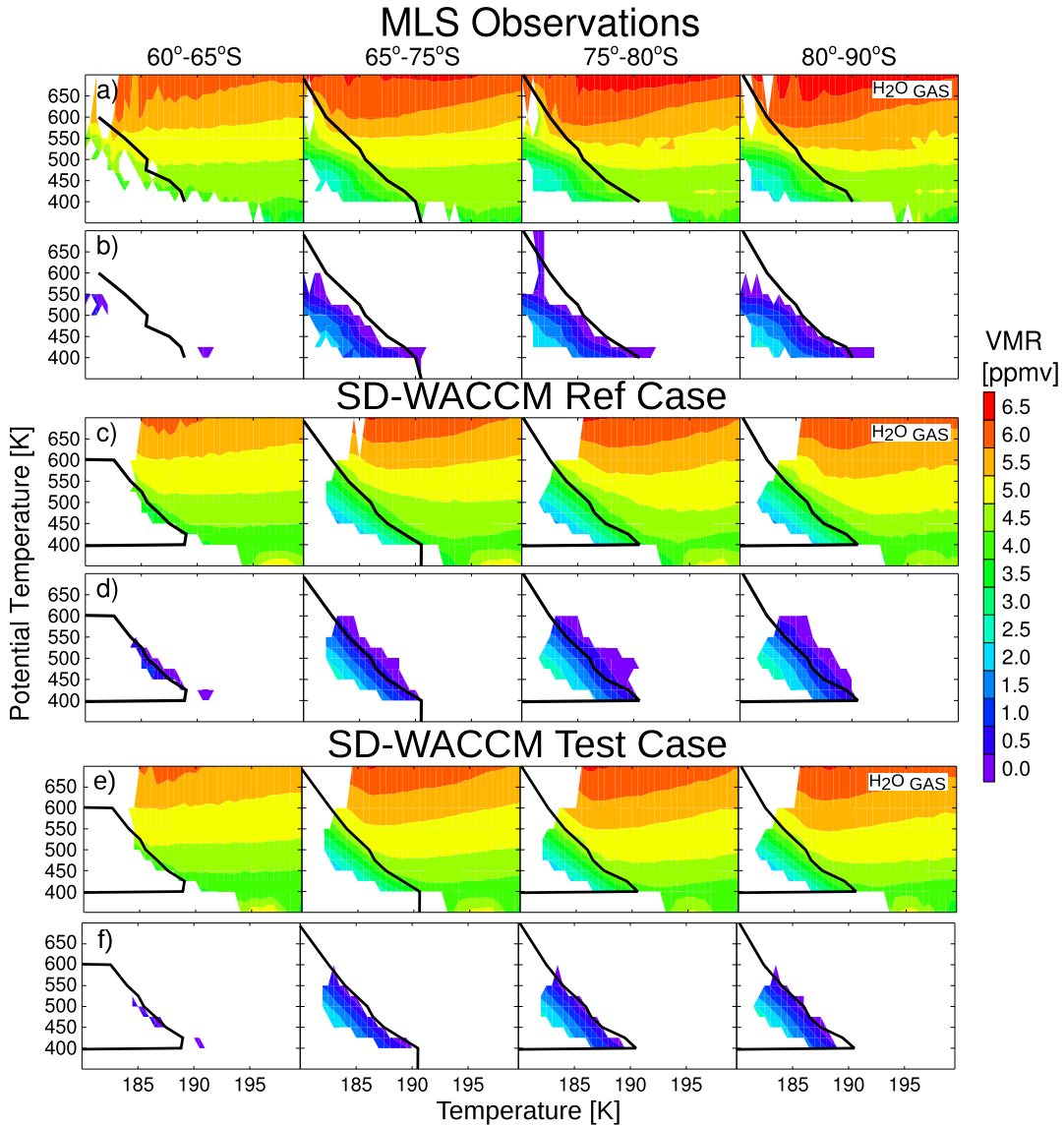
[27] The vertical distribution of HNO_3 generally shows improvement in the test simulation, especially in early winter (Figure 7). On 1 June, the reference simulation clearly underestimates gas-phase HNO_3 over the entire vertical

range. The vertical distribution of the simulation with the new PSC scheme, on the other hand, shows excellent agreement with the observations. The test case can reproduce the absolute numbers of the observations as well as the vertical structure with two maxima at 425 and 600 K, respectively. Only from August, onward and below 500 K is the reference simulation in better agreement with the observations than the test case. Although gas-phase HNO_3 in the test simulation tends to be higher than the observations, the shapes of the vertical distributions are in agreement.

Figure 8. (a) All MLS gas-phase H_2O observations on 475 K between 1 May and 1 July 2005 poleward of 80°S correlated with temperature. (b) Reference simulation output co-located with the observations described in Figure 8a. (c) Same as Figure 8b for the test simulation. Solid blue line marks T_{ICE} which is calculated separately for model and observations with mean water vapor between 195 and 200 K on 475 K poleward of 80°S EqL.
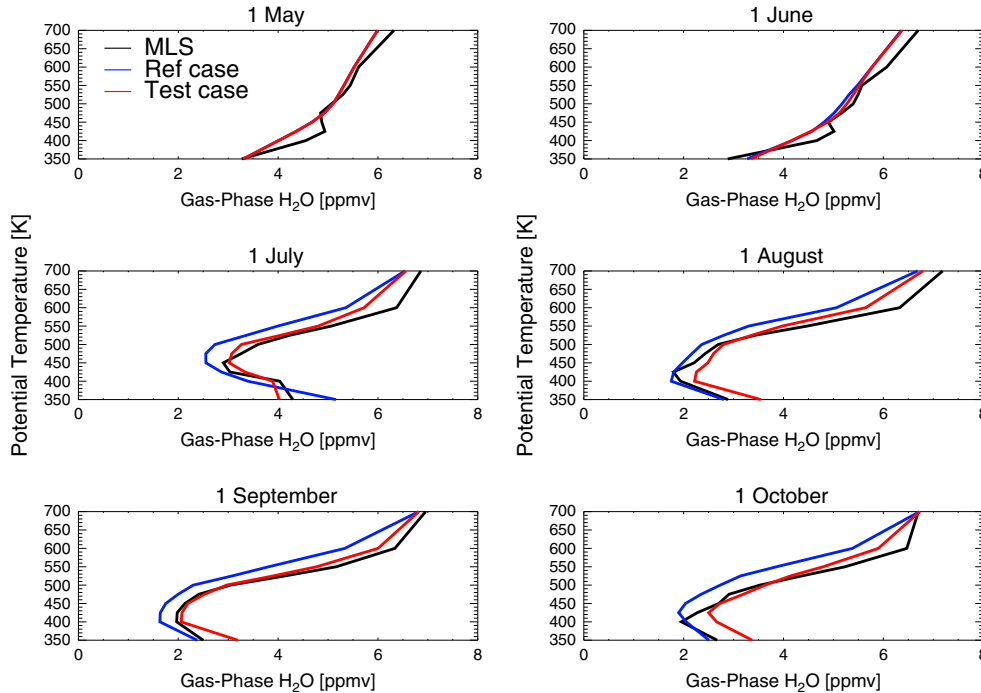
Figure 9. (a) All vertical profiles of MLS gas-phase H_2O observations between 1 May to 1 July 2005 averaged in 1 K temperature intervals for four equivalent latitude regions in potential temperature space. (b) Difference between the observed vertical distribution of H_2O at a given temperature, shown in row of Figure 9a, and the initial vertical distribution. Initial H_2O is the mean vertical distribution of gas-phase H_2O between 195 and 200 K temperature. (c) Same as Figure 9a for gas-phase H_2O in the reference simulation. (d) Same as Figure 9b for the reference simulation. (e) Same as Figure 9a for the test simulation. (f) Same as Figure 9b for the test simulation. Solid line marks T_{ICE}, calculated as described in Figure 3.

Gas-phase HNO_3 in the test simulation, except for the initialization on 1 May, never exceeds the observations by more than 2 ppbv, while the reference simulation is, temporarily, more than 5 ppbv lower than the observations.

[28] Overall, the test simulation is in better agreement with observations than the reference although it never completely removes HNO_3 from the gas phase. The test case can reproduce the observations in terms of irreversible denitrification at the end of polar night and the vertical distribution of gas-phase HNO_3 during the entire winter; furthermore, its distribution of PSCs and the transition between the different PSC types also agrees with theory and observations.

4. Type II PSCs

[29] A second type of PSCs are clouds composed of ice particles which can form at temperatures below the frost point (T_{ICE}). These low temperatures are usually only observed in the Antarctic stratosphere and mountain waves [*Carslaw et al.*, 1998]; however, some winters in the Arctic, e.g., 2009/2010, also exhibited temperatures below the frost point, leading to the formation of ice PSCs on synoptic scales [*Pitts et al.*, 2011; *Khosrawi et al.*, 2011]. Analogous to NAT causing irreversible denitrification, ice PSCs lead to irreversible dehydration of the stratosphere. While ice PSCs do provide additional surface area for heterogeneous

Figure 10. Average vertical distribution of gas-phase H_2O for six different days in 2005 poleward of 80°S EqL. Solid black lines are the MLS measurements, blue lines are the reference simulation, and red lines are the test simulation with updated PSC scheme.

reactions, by the time this type of cloud forms, heterogeneous chemistry on other PSC types is already fast enough that the additional surface area has no significant effect on the abundance of activated chlorine. However, the abundance of water vapor is the principal factor determining the solubility of trace gases in STS droplets. The solubility of HNO_3 and HCl as parameterized in *Carslaw et al.* [1995b] is primarily a function of water activity. With water vapor tied up in ice, less water condenses onto STS which causes a drastic decrease in HCl and HNO_3 solubility. For example, at 186 K and 50 hPa, a drop in gas phase water vapor from 4.5 to 2 ppmv, which commonly occurs in the Antarctic, causes the fraction of dissolved HNO_3 to drop from 99 to 75% and HCl from 76 to 1%. Therefore, an accurate representation of ice PSCs is necessary to simulate the composition of STS droplets.

4.1. Observations and Reference Simulation

[30] Just as HNO_3 removal from the gas phase can serve as an indicator for the presence of STS and NAT, a decrease in water vapor indicates the presence of ice clouds. The temperature dependence of water vapor observations by MLS (Figure 8a) shows that water vapor starts to decrease around the frost point (T_{ICE}), as defined according to *Marti and Mauersberger* [1993]. In the reference simulation, in contrast to the observations, water vapor starts to decrease about 2 K above the frost point.

[31] Water vapor observations from MLS indicate the presence of ice PSCs between 400 and 550 K poleward of 65°S equivalent latitude (Figures 9a and 9b). These observations indicate that ice PSCs below 500 K first occur at temperatures around T_{ICE}, which means that no or only little supersaturation is needed for ice clouds to form.

With increasing altitude, MLS only observes a decrease in water vapor at temperatures well below the frost point, indicating that here some supersaturation is needed before ice clouds form. This is in agreement with the laboratory results of *Koop et al.* [1998] and may be explained by a change in the abundance and composition of nonvolatile particles which can act as condensation nuclei [*Murphy et al.*, 1998, 2007]. The highest altitude for the presence of ice PSCs as observed by MLS appears to be between 550 and 600 K (26–28 km). SD-WACCM, like many other models, assumes that ice clouds are always in equilibrium with water vapor, and their formation is controlled by a parameter that is connected to the relative humidity. In the reference simulation, ice clouds form up to 600 K and remove water from the gas phase faster than is observed. Observations show a decrease in water vapor by the end of June of up to 50% (2 ppmv) in the vortex core (Figure 9b), while in the model, water vapor decreases by up to 3 ppmv.

4.2. PSC Type II Test Simulation With an Improved PSC Scheme

[32] The parameter controlling the formation of ice clouds in the reference simulation was set, so that modeled upwelling of water vapor through the cold point near the tropical tropopause agrees with observations. To achieve an improved representation of ice clouds in the Antarctic vortex, this parameter was tuned in the test case so that ice clouds form at temperatures close to the frost point.

[33] With this tuned parameter, water vapor in the test simulation is in better agreement with observations (Figure 8c) than the reference simulation. Water vapor still starts to decrease at temperatures slightly above the frost point, but the modeled temperature dependence is close to

observations by MLS. The modeled temperature dependence of water vapor shows less scatter than the observations, due to the assumption that all ice clouds are in instant thermodynamic equilibrium with the gas phase. In the real atmosphere ice formation, just like NAT formation, probably depends on more factors than just the equilibrium temperature leading to variable attributes of the ice cloud (e.g., size distribution and particle number density). This variability and the accuracy of the observations probably cause the scatter of the temperature dependence.

[34] In the test simulation, the onset of ice formation over the whole vertical range occurs close to the frost point (Figure 9e), in agreement with observations. But the gradient of water vapor with decreasing temperature is stronger in the model than in the observations. At the minimum temperature on the 500 K isentrope, observations show a decrease in water vapor of 1.5 ppmv (Figure 9b), while the test simulation shows a decrease of 2.5 ppmv, although temperatures in the model are about 1.5 K higher than the observations indicate.

[35] The vertical distributions of water vapor over the Antarctic winter 2005 for our simulations and observations are shown in Figure 10. The test simulation reproduces the shape of the MLS observations. While the reference simulation underestimates the abundance of water vapor over the whole vertical range by about 0.5–1 ppmv, the test case gives a better representation of observed water vapor over the entire lower stratosphere and throughout the entire winter. The vertical distribution on 1 October indicates the extent of irreversible dehydration since PSCs are no longer present at this time. Above 450 K, the reference simulation overestimates irreversible dehydration by about 0.5–1 ppmv, while the test simulation is in excellent agreement with observations. Since the vertical distribution barely changes between 1 August and 1 October, we can assume that a large part of irreversible dehydration has occurred by 1 August.

5. Conclusions

[36] Observations from MLS provide important constraints on the occurrence of PSCs in the Antarctic winter of 2005 and their representation in climate models. Our analysis focuses on the months of May and June, which provide information on the beginning of the PSC formation phase. Observations show that gas-phase HNO_3 decreases between T_{S_NAT} and T_{ICE}. Most of this decrease can be explained with condensation of HNO_3 on the background aerosol and the subsequent formation of STS. But around the 500 K isentrope, HNO_3 decreases at temperatures where no significant uptake of HNO_3 on the background aerosol is expected. At this altitude, HNO_3 may be nucleating to NAT clouds with high particle number densities which can deplete gas-phase HNO_3 on a short timescale. Besides STS and NAT, we show observations of ice clouds that coincide with temperatures around the frost point.

[37] We explore how well a model with a simplified PSC scheme can represent the observed removal of HNO_3 and H_2O from the gas phase. The reference simulation has a fairly good representation of overall denitrification at the end of winter. However, the reference simulation also has a sharp transition from NAT to STS with decreasing temperature with almost no occurrence of mixed PSCs. In contrast,

observations show that PSCs transition from STS to NAT with decreasing temperature, with liquid PSCs being the dominant type, and a large fraction consisting of mixed PSCs. For our test simulation, only a certain fraction of total HNO_3 is allowed to form NAT, which forces the formation of mixed PSCs in the model. This approach significantly improves the agreement of the model with observations. In particular, the temperature dependence of HNO_3 removal from the gas phase now shows good agreement with observations by MLS. With a NAT particle number density of 10^{-2} cm^{-3}, the modeled denitrification agrees with observations while also giving an improved representation of HNO_3 containing PSCs. Most importantly, the unphysical transition from solid to liquid particles with decreasing temperature is removed in the test case, and mixed phase PSC occur throughout the entire winter.

[38] MLS observations show an initial decrease of water vapor at temperatures around the frost point, which suggests that no or only slight supersaturation is needed to form ice PSCs in the polar stratosphere. The reference simulation uses a global parameter to specify the needed supersaturation for ice clouds, which was derived according to the upwelling of water vapor through the tropopause. But this approach forms ice clouds at temperatures well above the frost point, which causes a faster decrease of water vapor compared to observations. In the test case, ice clouds form closer to the frost point, which gives better agreement with the observed temperature dependence and vertical distribution of water vapor. It also improves the agreement between model and observations in terms of irreversible dehydration at the end of winter.

[39] Since ice clouds near the tropical cold point and the polar stratosphere appear to require different supersaturation for their formation, ice clouds in these two regions may have different nucleation mechanisms. *Murphy et al.* [1998, 2007] reported an altitude dependence in the abundance and composition of nonvolatile material in aerosols. Different nonvolatile particles can also have very different capabilities to act as condensation nuclei. This may explain an altitude dependence for the formation of ice clouds. But without coupling SD-WACCM to a microphysical model, this behavior cannot be accurately represented. Overall, the model gives a good representation not only of PSC composition but also of irreversible denitrification and dehydration with the changes in parameterization described here, despite the simplified assumption that all PSCs form instantaneously and independent of the air's history. Since the computational effort for the reference and the improved PSC scheme are practically identical, the new parameterization will be used in decadal and free-running simulations of WACCM.

References

Adriani, A., P. Massoli, G. Di Donfrancesco, F. Cairo, M. L. Moriconi, and M. Snels (2004), Climatology of polar stratospheric clouds based on lidar observations from 1993 to 2001 over McMurdo Station, Antarctica, *J. Geophys. Res.*, *109*, D24211, doi:10.1029/2004JD004800.

Biele, J., A. Tsias, B. P. Luo, K. S. Carslaw, R. Neuber, G. Beyerle, and T. Peter (2001), Nonequilibrium coexistence of solid and liquid particles in Arctic stratospheric clouds, *J. Geophys. Res.*, *106*, D19, doi:10.1029/2001JD900188.

Butchard, N., and E. E. Remsberg (1986), The area of the stratospheric polar vortex as a diagnostic for tracer transport on an isentropic surface, *J. Atmos. Sci.*, *43*, 1319–1339, doi:10.1175/1520-0469(1986)043<1319:TAOTSP>2.0.CO;2.

Carslaw, K. S., B. P. Luo, S. L. Clegg, T. Peter, P. Brimblecombe, and P. J. Crutzen (1994), Stratospheric aerosol growth and HNO₃ gas phase depletion from coupled HNO₃ and water uptake by liquid particles, *Geophys. Res. Lett.*, *21*, 2479–2482.

Carslaw, K. S., B. Luo, and T. Peter (1995a), An analytic expression for the composition of aqueous HNO₃-H₂SO₄ stratospheric aerosols including gas phase removal of HNO₃, *Geophys. Res. Lett.*, *22*, 1887–1880.

Carslaw, K. S., S. L. Clegg, and P. Brimblecombe (1995b), A thermodynamic model of the system HCl-HNO₃-H₂SO₄-H₂O, including solubilities of HBr, from <200 to 328 K, *J. Phys. Chem.*, *99*, 11,557–11,574, doi:10.1021/j100029a039.

Carslaw, K. S., M. Wirth, A. Tsias, B. P. Luo, A. Dörnbrack, M. Leutbecher, H. Volkert, W. Renger, J. T. Bacmeister, and T. Peter (1998), Particle microphysics and chemistry in remotely observed mountain polar stratospheric clouds, *J. Geophys. Res.*, *103* (D5), 5785–5796, doi:10.1029/97JD03626.

Davies, S., G. W. Mann, K. S. Carslaw, M. P. Chipperfield, J. J. Remedios, G. Allen, A. M. Waterfall, R. Spang, and G. C. Toon (2006), Testing our understanding of Arctic denitrification using MIPAS-E satellite measurements in winter 2002/2003, *Atmos. Chem. Phys.*, *6*, 3149–3161.

Drdla, K., R. P. Turco, and S. Elliott (1993), Heterogeneous chemistry on Antarctic polar stratospheric clouds: A microphysical estimate of the extent of chemical processing, *J. Geophys. Res.*, *98*, 8965–8981, doi:10.1029/93JD00164.

Dye, J. E., D. Baumgardner, B. W. Gandrud, S. R. Kawa, K. K. Kelly, M. Loewenstein, G. V. Ferry, K. R. Chan, and B. L. Gary (1992), Particle size distributions in arctic polar stratospheric clouds, growth and freezing of sulfuric acid droplets, and implications for cloud formation, *J. Geophys. Res.*, *97*, 8015–8034.

Emmons, L. K., et al. (2010), Description and evaluation of the Model for Ozone and Related chemical Tracers, version 4 (MOZART-4), *Geosci. Model Dev.*, *3*, 43–67, doi:10.5194/gmd-3-43-2010.

Eyring, V., T. G. Sheperd, and D. W. Waugh (eds.) (2010), SPARC report on the evaluation of chemistry-climate models, *SPARC Rep. No. 5, WRCP-132, WMO-TD No. 1526*, World Meteorol. Organ., Geneva.

Fahey, D. W., et al. (2001), The detection of large HNO₃-containing particles in the winter Arctic stratosphere, *Science*, *291*, 1026–1031, doi:10.1126/science.1057265.

Feng, W., M. P. Chipperfield, S. Davies, G. W. Mann, K. S. Carslaw, S. Dhomse, L. Harvey, C. Randall, and M. L. Santee (2011), Modeling the effect of denitrification on polar ozone depletion for Arctic winter 2004/2005, *Atmos. Chem. Phys.*, *11*, 6559–6573, doi:10.5194/acp-11-6559-2011.

Garcia, R. R., D. Marsh, D. E. Kinnison, B. Boville, and F. Sassi (2007), Simulation of secular trends in the middle atmosphere, 1950–2003, *J. Geophys. Res.*, *112*, D09301, doi:10.1029/2006JD007485.

Grooß, J.-U., G. Günther, R. Müller, P. Konopka, S. Bausch, H. Schlager, C. Voigt, C. M. Volk, and G. C. Toon (2005), Simulation of denitrification and ozone loss for the Arctic winter 2002/2003, *Atmos. Chem. Phys.*, *5*, 1437–1448.

Hanson, D. R., and K. Mauersberger (1988), Laboratory studies of the nitric acid trihydrate: Implications for the south polar stratosphere, *Geophys. Res. Lett.*, *15*, 855–858.

Kelly, K. K., et al. (1989), Dehydration in the lower Antarctic stratosphere during late winter and early spring, 1987, *J. Geophys. Res.*, *94*, 11,317–11,357, doi:10.1029/JD094iD09p11317.

Khosrawi, F., J. Urban, M. C. Pitts, P. Voelger, P. Achtert, M. Kaphlanov, M. L. Santee, G. L. Manney, D. Murtagh, and K.-H. Fricke (2011), Denitrification and polar stratospheric cloud formation during the Arctic winter 2009/2010, *Atmos. Chem. Phys.*, *11*, 8471–8487, doi:10.5194/acp-11-8471-2011.

Kinnison, D. E., et al. (2007), Sensitivity of chemical tracers to meteorological parameters in the MOZART-3 chemical transport model, *J. Geophys. Res.*, *112*, D20302, doi:10.1029/2006JD007879.

Koop, T., H. P. Ng, L. T. Molina, and M. J. Molina (1998), A new optical technique to study aerosol phase transitions: The nucleation of ice from H₂SO₄ aerosols, *J. Phys. Chem. A*, *102*, 8924–8931, doi:10.1021/jp9828078.

Kunz, A., L. Pan, P. Konopka, D. E. Kinnison, and S. Tilmes (2011), Chemical and dynamical discontinuity at the extratropical tropopause based on START08 and WACCM analysis, *J. Geophys. Res.*, *116*, D24302, doi:10.1029/2011JD016686.

Lamarque, J.-F., et al. (2012), CAM-chem: Description and evaluation of interactive atmospheric chemistry in the Community Earth System Model, *Geosci. Model Dev.*, *5*, 369–411, doi:10.5194/gmd-5-369-2012.

Lambert, A., et al. (2007), Validation of the Aura Microwave Limb Sounder middle atmosphere water vapor and nitrous oxide measurements, *J. Geophys. Res.*, *112*, D24S36, doi:10.1029/2007JD008724.

Lambert, A., M. L. Santee, D. L. Wu, and J. H. Chae (2012), A-train CALIOP and MLS observations of early winter Antarctic polar stratospheric clouds and nitric acid in 2008, *Atmos. Chem. Phys.*, *12*, 2899–2931, doi:10.5194/acp-12-2899-2012.

Lowe, D., and A. R. MacKenzie (2008), Polar stratospheric cloud microphysics and chemistry, *J. Atmos. Solar-Terr. Phys.*, *70*, 13–40.

Marsh, D. R., R. R. Garcia, D. E. Kinnison, B. A. Boville, S. Walters, K. Matthes, and S. Solomon (2007), Modeling the whole atmosphere response to solar cycle changes in radiative and geomagnetic forcing, *J. Geophys. Res.*, *112*, D23306, doi:10.1029/2006JD008306.

Marti, J., and K. Mauersberger (1993), A survey and new measurements of ice vapor pressure at temperatures between 170 and 250 K, *Geophys. Res. Lett.*, *20*, 363–366, doi:10.1029/93GL00105.

Meilinger, S. K., T. Koop, B. P. Luo, T. Huthwelker, K. S. Carslaw, U. Krieger, P. J. Crutzen, and T. Peter (1995), Size-dependent stratospheric droplet composition in Lee wave temperature fluctuations and their potential role in PSC freezing, *Geophys. Res. Lett.*, *22*, 3031–3034, doi:10.1029/95GL03056.

Murphy, D. M., D. S. Thomson, and M. J. Mahoney (1998), In situ measurements of organics, meteoritic material, mercury, and other elements in aerosols at 5 to 19 kilometers, *Science*, *282*, 1664–1669, doi:10.1126/science.282.5394.1664.

Murphy, D. M., D. J. Cziczo, P. K. Hudson, and D. S. Thomson (2007), Carbonaceous material in aerosol particles in the lower stratosphere and tropopause region, *J. Geophys. Res.*, *112*, D04203, doi:10.1029/2006JD007297.

Peter, T., C. Brühl, and P. J. Crutzen (1991), Increase in the PSC-formation probability caused by high-flying aircraft, *Geophys. Res. Lett.*, *18*, 1465–1468, doi:10.1029/91GL01562.

Pitts, M. C., L. R. Poole, and L. W. Thomason (2009), CALIPSO polar stratospheric cloud observations: Second-generation detection algorithm and composition discrimination, *Atmos. Chem. Phys.*, *9*, 7577–7589.

Pitts, M. C., L. R. Poole, A. Dörnbrack, and L. W. Thomason (2011), The 2009–2010 Arctic polar stratospheric cloud season: A CALIPSO perspective, *Atmos. Chem. Phys.*, *11*, 2161–2177, doi:10.5194/acp-11-2161-2011.

Rienecker, M. M., et al. (2011), MERRA: NASA's modern-era retrospective analysis for research and applications, *J. Climate*, *24*, 3624–3648, doi:10.1175/JCLI-D-11-00015.1.

Santee, M. L., et al. (2007), Validation of the Aura Microwave Limb Sounder HNO₃ measurements, *J. Geophys. Res.*, *112*, D24S40, doi:10.1029/2007JD008721.

Schwartz, M. J., et al. (2008), Validation of the Aura Microwave Limb Sounder temperature and geopotential height measurements, *J. Geophys. Res.*, *113*, D15S11, doi:10.1029/2007JD008783.

Solomon, S., R. R. Garcia, F. S. Rowland, and D. J. Wuebbles (1986), On the depletion of Antarctic ozone, *Nature*, *321*, 755–758.

Tabazadeh, A., R. P. Turco, and M. Z. Jacobson (1994), A model for studying the composition and chemical effects of stratospheric aerosols, *J. Geophys. Res.*, *99*, 12,897–12,914.

Tilmes, S., D. E. Kinnison, R. R. Garcia, R. Müller, F. Sassi, D. R. Marsh, and B. A. Boville (2007), Evaluation of heterogeneous processes in the polar lower stratosphere in the Whole Atmosphere Community Climate Model, *J. Geophys. Res.*, *112*, D24,301, doi:10.1029/2006JD008334.

Waters, J. W., et al. (2006), The Earth Observing System Microwave Limb Sounder (EOS MLS) on the aura satellite, *IEEE Trans. Geosci. Remote Sens.*, *44*, 1075–1092, doi:10.1109/TGRS.2006.873771.

Waugh, D. W., and W. J. Randel (1999), Climatology of Arctic and Antarctic polar vortices using elliptical diagnostics, *J. Atmos. Sci.*, *56*, 1594–1613, doi:10.1175/1520-0469(1999)056<1594:COAAAP>2.0.CO;2.

Winker, D. M., M. A. Vaughan, A. Omar, Y. Hu, K. A. Powell, Z. Liu, W. H. Hunt, and S. A. Young (2009), Overview of the CALIPSO mission and CALIOP data processing algorithms, *J. Atmos. Oceanic Technol.*, *26*, 2310–2323, doi:10.1175/2009JTECHA1281.1.